RC24735 (W0901-020) January 7, 2009
Electrical Engineering

IBM Research Report

Area-of-Polygon Based Projection for Simulation and Reconstruction in Fan-Beam X-ray CT

Somesh Srivastava, Vadim Sheinin
IBM Research Division
Thomas J. Watson Research Center
P.O. Box 218
Yorktown Heights, NY 10598

Research Division
Almaden - Austin - Beijing - Cambridge - Haifa - India - T. J. Watson - Tokyo - Zurich

AREA-OF-POLYGON BASED PROJECTION FOR SIMULATION AND RECONSTRUCTION IN FAN-BEAM X-RAY CT

Somesh Srivastava, Member, IEEE, Vadim Sheinin, Senior Member, IEEE

Multimedia technologies department, IBM T.J.Watson Research Center
1101 Kitchawan Rd, Route 134, Yorktown Heights, NY, USA. 10598.

ABSTRACT

A novel method to simulate a fan-beam X-ray computed tomography (CT) scanner in a digital computer is presented in this paper. The line integral along a ray through the object is computed by splitting the overlap between the ray and the pixellated object into polygons. The line integral is then computed as a weighted sum of areas of these polygons, where the weights convert the areas into line-lengths. To reconstruct the object from the raw data produced by the above simulator, we use a statistical image reconstruction algorithm to produce a noise-free image. The forward projector used in the algorithm is computed using a method similar to that used in the simulator, but approximate areas are used instead to reduce reconstruction time. The main motivation behind the proposed forward projector is to model the scanner as accurately as possible for applications that demand highly accurate reconstructions, e.g. removal of calcium blooming artifacts in cardiac scans.

Index Terms— X-ray computed tomography, statistical image reconstruction algorithms, simulator, projector

1. INTRODUCTION

X-ray CT is one of the most commonly used medical imaging modalities for diagnosing patients. The traditional method to reconstruct images from the raw data obtained from an X-ray CT scanner is Filtered backprojection (FBP). But, due to the need to reduce patient-dose and to scan with non-standard geometries, like those that arise during cardiac scans, statistical image reconstruction algorithms (or, algorithms, for short) are being developed [1]. To develop new algorithms that target particular image artifacts, e.g. calcium blooming [2, 3], it is necessary to produce the raw data in a controlled environment. An X-ray CT simulator serves this purpose very well, even though it is not a replacement for the actual scanner. In an actual scanner, many physical phenomena act simultaneously which makes the study of a particular phenomenon hard.

X-ray CT scanners have been simulated in the past and a recent effort can be found in De Man *et al.*, SPIE 2007, vol. 6510. To reconstruct objects using statistical methods, various methods of projection have been proposed, which include ray-driven, pixel-driven, and distance-driven methods [4]. Many of these methods employ the Siddon's algorithm ([5] and Siddon '85) to compute the intersection points between a rectangular cartesian grid and a straight line. Many physical effects are active in a X-ray CT scanner, of which we simulate the following: detector noise, polychromatic nature of the X-ray beam, partial-volume effect, and finite spot-size.

This paper is organized as follows. Section 2 describes the model of the scanner used to generate the raw sinogram data. Section 3 describes the proposed projection method for simulation and reconstruction. Section 4 describes the statistical image reconstruction algorithm used in this paper. Section 5 discusses the experimental setup, and Section 6 presents the results. Section 7 presents the conclusions and future work.

2. SCANNER MODEL

The fan-beam X-ray CT scanner is made up of a X-ray source of a finite spot-size and an arc-detector array whose focal point coincides with the center of the source. The finite extent of the X-ray source is modeled as a line-segment. Every point on the detector element receives photons from every point on the source. Thus, if we divide the source and the detector element into infinitesimally small segments, we can decompose a single detector measurement, y_i, into rays connecting every section of the source with every section of a detector element. This set of rays is called $\mathcal{I}_i$. However, during simulation, for practical reasons, we divide the source and detector elements into only a finite number of segments (4 each, in this paper) instead of having an infinite number of such infinitesimally small segments. The object being scanned is assumed to be a pixelized image that is made up of two kinds of tissue: soft-tissue and bone (calcium beads). The signal generated at the ith detector, y_i, is assumed to be a Poisson random variable:

$$y_i \sim \text{Poisson}(\sum_{i' \in \mathcal{I}_i} (b_{i'} e^{-f(T_{S,i'}, T_{B,i'})}) + r_i),$$

Somesh Srivastava is a post doctoral researcher in, and Vadim Sheinin is the manager of, the Multimedia technologies department at the IBM T.J. Watson research center. They can be reached at `srivasts@us.ibm.com` and `vadims@us.ibm.com` respectively.

$$f(T_{S,i'}, T_{B,i'}) \triangleq \ln \frac{b_{i'}}{\int I_{i'}(\mathcal{E}) e^{(-m_S(\mathcal{E})T_{S,i'} - m_B(\mathcal{E})T_{B,i'})} d\mathcal{E}},$$

$$T_{S,i'} \triangleq \int_{L_{i'}} F_S(\boldsymbol{r})\rho(\boldsymbol{r})d\boldsymbol{r},\ T_{B,i'} \triangleq \int_{L_{i'}} F_B(\boldsymbol{r})\rho(\boldsymbol{r})d\boldsymbol{r},$$

$$b_{i'} \triangleq \int I_{i'}(\mathcal{E})d\mathcal{E},\ \rho(\boldsymbol{r}) \triangleq \sum_{j,k} \rho_{j,k}\alpha_{j,k}(\boldsymbol{r}),$$

where, $I_{i'}(\mathcal{E})$ is the spectrum of the i'th ray exiting the source, $m_S(\mathcal{E})$ and $m_B(\mathcal{E})$ are spectral responses of soft-tissue and bone resp., $T_{S,i'}$ and $T_{B,i'}$ are line-integrals through soft-tissue and bone resp. along the i'th ray, $b_{i'}$ is the total number of photons exiting the source in ray i', r_i represents photon counts attributed to scatter, electronic noise etc. (LaRiviere '06), $f(T_S, T_B)$ maps the water and bone line-integrals in a ray into the attenuation experienced by it, F_S and F_B segment the object into soft-tissue and bone considering the partial-volume effect, $\rho(\boldsymbol{r})$ is the distribution of material density in the object, and $\alpha_{j,k}(\boldsymbol{r})$ is the pixel-basis here. Note that the line-integrals $T_{S,i'}$ and $T_{B,i'}$ are finite sums over the basis coefficients $\rho_{j,k}$.

3. PROPOSED PROJECTION METHOD

A ray $i' \in \mathcal{I}_i$ is shown in Fig. 1. To compute a line-integral (*i.e.* $T_{S,i'}$ or $T_{B,i'}$) along this ray, it is further subdivided into trapezoidal sections. The parallel sides of the trapezoids are parallel to the detector element. l_n is the height of the nth trapezoid. Thus, the line-integral is the sum over n of l_n multiplied by the average material density within the trapezoid. l_n is calculated by noting that the area, A_n, of a trapezoid is the product of l_n and the average of its parallel sides, W_n. For a pixelized image, A_n is the sum of areas of individual polygons (*e.g.*, $A_n = A_{n,1} + A_{n,2} + A_{n,3} + A_{n,4}$ in Fig. 1). Thus, the coefficient in the forward projection matrix corresponding to pixel (n, m) and ray i' would be $A_{n,m}/W_n$ [1]. Note that this method of computing the line-integral can be used even when the spot-size is zero.

During simulation, $A_{n,m}$ is calculated exactly by first determining the v vertices of the corresponding polygon, $\{(x_j, y_j) : j = 0, \ldots, v-1\}$, using the Siddon's algorithm [5]. Then, the v vertices are sorted in a counterclockwise order, and the formula $A = \sum_{j=0}^{v-1}(x_j y_{j+1} - x_{j+1}y_j)$, where $x_v = x_0, y_v = y_0$ (from elementary cartesian geometry) is used to calculate $A_{n,m}$. W_n is calculated as the width of the ray i' around pixel (n, m). The number of mathematical operations required to compute l_n in this manner is very high when compared to the currently used simpler projection operations, like the ones mentioned in Section 1.

During reconstruction, the above idea is modified to trade-off reconstruction time and accuracy as follows. The area of the polygon corresponding to pixel (n, m) and ray i' is computed by approximating the polygon as a trapezoid (Fig. 2). The area is computed as the product of pixel height multiplied by overlap width, D^{approx}, at the center of the pixel. For many of the cases (roughly one-third), the area computed this way exactly equals the actual area. This method is reminiscent of the distance-driven method, but a line parallel to the x-axis and passing through the center of a pixel is used as the common axis instead of the x-axis [4].

The reconstruction can be done at many levels of geometric accuracy depending on the number of segments into which the source and detector elements are subdivided. But, this type of investigation is left for the future. Instead, two simple projectors for reconstruction are explored here: zero spot-size (ZS) and finite spot-size (FS). In the ZS projector, the source is assumed to be of zero size and the detector elements are not subdivided (projectors used currently assume a zero spot-size). In the FS projector, the source and detector elements have their respective original sizes and are not subdivided.

There is a mismatch in the geometries of both ZS and FS projectors and the simulator. Thus, the raw data produced by the simulator will need to be modified for reconstruction. During experimentation, it was found that the FS projector does not require any modification of the observed line-integrals (*i.e.* $ln(b_i/(y_i - r_i)), b_i \triangleq \sum_{i' \in \mathcal{I}_i} b_{i'}$). The raw data is modified for the ZS projector as follows. We construct an image that has the shape of the object and the attenuation at all pixels is equal to that of water (1000 HU). The FBP image is thresholded at 70 HU to obtain this image. This image is forward projected with ZS and FS projectors, and the ratio of the two sinograms gives us a scaling sinogram. The observed line-integrals are then multiplied by the scaling sinogram and used with the reconstructor employing the ZS projector.

The number of computations involved in the ZS projector are half of that of FS, but it is less faithful to the simulator geometry.

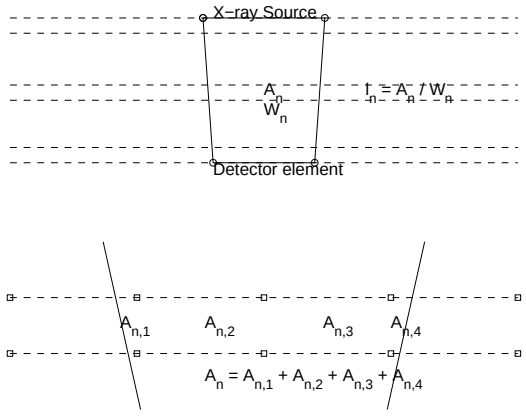

Fig. 1. Proposed method for forward projection.

[1] To keep computations simple, we use the lines of the cartesian grid as the parallel sides of the trapezoidal sections. As a result, in the implementation, W_n becomes dependent on m also. This approximation works well in experiments.

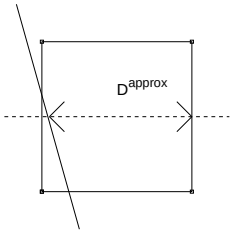

Fig. 2. Approximate area calculation for reconstruction.

4. STATISTICAL IMAGE RECONSTRUCTION ALGORITHM

The statistical image reconstruction algorithm employs a penalized weighted least squares (PWLS) cost function, $\Phi(\boldsymbol{\mu})$, to reconstruct the image of X-ray attenuation coefficients, $\boldsymbol{\mu}$:

$$\Phi(\boldsymbol{\mu}) = -L(\boldsymbol{\mu}) + \beta R(\boldsymbol{\mu}), -L(\boldsymbol{\mu}) = \sum_{i=1}^{n_d} \tfrac{1}{2} w_i ([\boldsymbol{G}\boldsymbol{\mu}]_i - l_i)^2,$$

where, $-L(\boldsymbol{\mu})$ is the negative log-likelihood function, n_d is the number of sinogram bins, l_i and w_i are parameters derived from y_i (see below), $\boldsymbol{G}$ is the forward projector (either ZS or FS), $R(\boldsymbol{\mu})$ is an edge-preserving regularization function (see Fessler and Booth '99), and β is the regularization parameter. The parameters l_i and w_i are computed from y_i as follows:

$$l_i = f_S^{-1}(\ln(\frac{b_i}{y_i - r_i})),\ w_i = (\frac{df_S}{dT_S}(l_i))^2 \frac{(y_i - r_i)^2}{y_i},$$

where, $f_S(T_S) \stackrel{\triangle}{=} f(T_S, 0)$, $b_i \stackrel{\triangle}{=} \sum_{i' \in \mathcal{I}_i} b_{i'}$. Only water-correction of the observed line-integrals is performed to have a simple cost function and algorithm. The algorithm used to minimize $\Phi(\boldsymbol{\mu})$ is an unconstrained preconditioned conjugate gradient (PCG) algorithm defined in Fessler and Booth '99, Eqs. 6,7,34. Diagonal preconditioner and restarting every 30 iterations are used with the algorithm.

5. EXPERIMENTAL SETUP

The simulation setup is as follows. The digital object phantom is a modified shepp-logan phantom occupying an ellipse of major and minor diameters 34 and 25 cm resp., and is made of soft-tissue. 6 calcium beads of varying diameters and contrasts are embedded in the soft-tissue ellipse. F_S and F_B are binary masks. This object occupies a 1024×1024 square grid with a pixel size 0.56mm. The X-ray source is 540mm from the origin and the center of the detector array is 410mm from the origin. There are 444 detector elements in the detector array, each of length 2mm. The spot-size of the X-ray source is 2.4mm. The observations are collected over 360° with 492 views. During simulation, the source and detector are further subdivided into 4 segments each. For each ray, $b_i = 2 \times 10^6$ and $r_i = 200$.

The reconstruction grid is 256×256 with square pixel size 2.26mm. Two reconstructions using the PCG algorithm employing either the ZS or the FS projectors were obtained. 180 iterations of the PCG algorithm with 3 regularization sub-iterations were run. Maximum absolute difference between consecutive iterations at the 179th iteration was less than 1 HU in both cases. The input line-integrals to the FBP algorithm were a constant multiplied with the output of the simulator. This constant made the FBP match the brightness of the true image.

The forward and back projectors for reconstruction, and the forward projector for the simulator were implemented using C and Message passing interface (MPI). Fessler's open source and free, Image reconstruction toolbox (IRT) (http://www.eecs.umich.edu/∼fessler) was used for the beam-hardening information, fan-beam FBP algorithm, regularization, and the PCG image reconstruction algorithm. A dual-core Intel machine containing the Core 2 Duo processor running at 3GHz and 3GB RAM was used. The time taken to perform one FS forward projection and one simulator forward projection were 30seconds and 2 hours approximately. The ZS forward projection is currently implemented using an FS implementation and takes the same time as the FS forward projection. In future, a much faster ZS implementation can be developed.

6. RESULTS AND DISCUSSION

Fig. 3 shows the true image (downsampled), FBP, ZS and FS reconstructions. Fig. 4 shows the image profile along a horizontal line that passes through the two highest calcium beads. These two figures show that FBP, ZS and FS reconstructed the true image well, except for the calcium beads. The image regions around the calcium beads are not reconstructed well by the statistical algorithms due to their sensitivity to the mismatch between the cost function used during reconstruction and the actual physical processes producing the raw data (*i.e.* model mismatch). FBP appears to be less sensitive to the model mismatch around the calcium beads. But, noise properties of ZS and FS are much better than those of FBP. This advantage of statistical algorithms will be crucial when observations with lower counts per ray will be used. Fig. 5 compares the ZS and FS reconstructions. We find that even though both ZS and FS have errors around calcium beads due to model mismatch, FS performs much better. Aliasing artifacts are seen near the soft-tissue and air boundary, and these are lower in the FS case.

7. CONCLUSIONS AND FUTURE WORK

The simulator emulates an actual scanner well (upto a scale factor), as is evident from the accurate FBP reconstruction. The ZS and FS projectors allow the PCG algorithm to reconstruct the true image accurately. The FS projector pro-

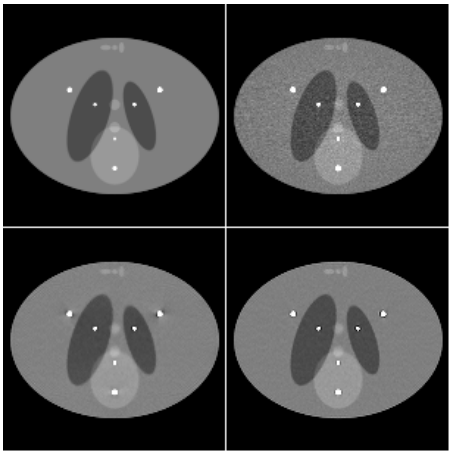

Fig. 3. Image reconstructions (window = 400 HU). Clockwise from top left: true (downsampled), FBP, FS, ZS).

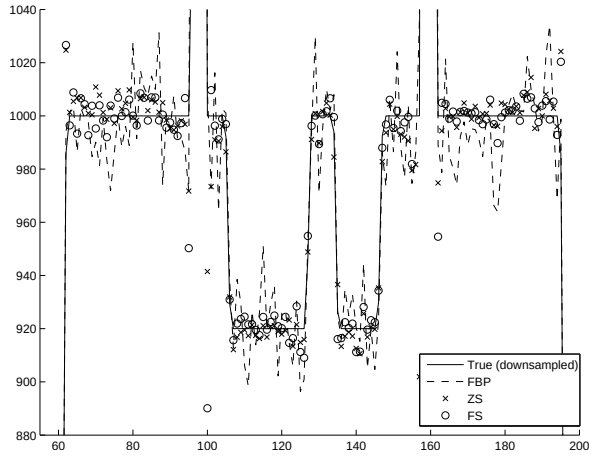

Fig. 4. Image profiles along the two vertically highest calcium beads.

vides a better reconstruction than the ZS projector, though at a higher computational cost. Image artifacts due to model mismatch around the calcium beads need to be removed. For this, the statistical image reconstruction algorithm will probably require modifications pertaining to the geometry (*i.e.* further subdivision of source and detector elements), the beam-hardening model, and the partial-volume effect. Finally, the projectors developed here need to be tested with raw data from an actual scanner.

8. REFERENCES

[1] J-B. Thibault, K. Sauer, C. Bouman, and J. Hsieh, "A three-dimensional statistical approach to improved image quality for multi-slice helical CT," *Med. Phys.*, vol. 34, no. 11, pp. 4526–44, Nov. 2007.

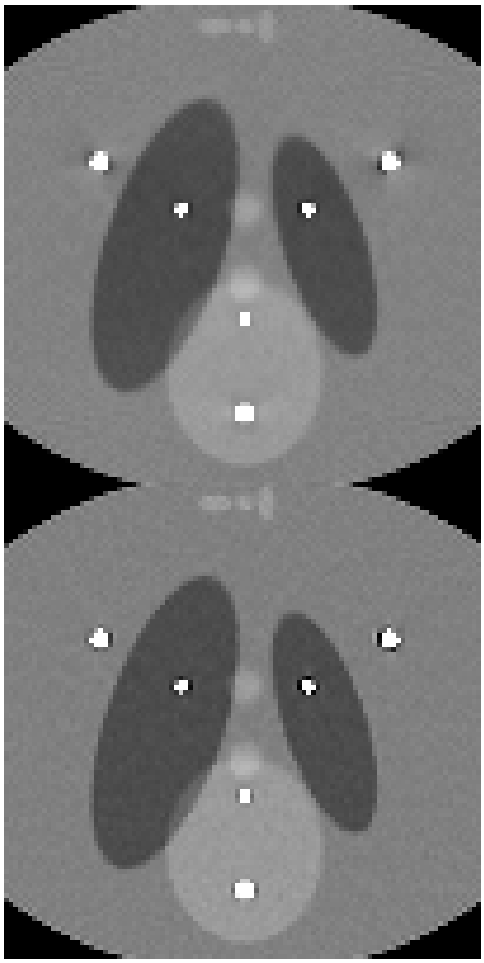

Fig. 5. Comparison of ZS (top) and FS (bottom) images (window = 400 HU).

[2] Zhuangli Liang, W.C. Karl, Synho Do, U. Hoffmann, T. Brady, and H. Pien, "Calcium de-blooming in coronary ct image," *Bioinformatics and Bioengineering, 2007. BIBE 2007. Proceedings of the 7th IEEE International Conference on*, pp. 257–262, Oct. 2007.

[3] J. Dehmeshki, Xujiong Ye, H. Amin, M. Abaei, XinYu Lin, and S.D. Qanadli, "Volumetric quantification of atherosclerotic plaque in ct considering partial volume effect," *Medical Imaging, IEEE Transactions on*, vol. 26, no. 3, pp. 273–282, March 2007.

[4] B. De Man and S. Basu, "Distance-driven projection and backprojection in three dimensions," *Phys. Med. Biol.*, vol. 49, no. 11, pp. 2463–75, June 2004.

[5] F. Jacobs, E. Sunderman, B. De Sutter, M. Christiaens, and I. Lemahieu, "A fast algorithm to calculate the exact radiological path through a pixel of voxel space," *J. Computing Inform. Technology*, vol. 6, no. 1, pp. 89–94, 1998.